Stall force of polymerizing microtubules and filament bundles

J. Krawczyk and J. Kierfeld

Physics Department, TU Dortmund University, 44221 Dortmund, Germany, EU

Abstract. - We investigate stall force and polymerization kinetics of rigid protofilaments in a microtubule or interacting filaments in bundles under an external load force in the framework of a discrete growth model. We introduce the concecpt of polymerization cycles to describe the stochastic growth kinetics, which allows us to derive an exact expression for the stall force. We find that the stall force is independent of ensemble geometry and load distribution. Furthermore, the stall force is proportional to the number of filaments and increases linearly with the strength of lateral filament interactions. These results are corroborated by simulations, which also show a strong influence of ensemble geometry on growth kinetics below the stall force.

Introduction. – Polymerization of cytoskeletal filaments is essential for various cellular processes, such as motility or the formation of cellular protrusions including filopodia or lamellipodia [1, 2]. Single polymerizing filaments can generate forces in the piconewton range, as has been demonstrated experimentally for microtubules (MTs) [3]. Such force generation mainly relies on the gain in chemical bonding energy upon monomer attachment [4]. An opposing force slows down filament growth, which finally stops at the stall force representing the maximal polymerization force a filament can generate. Therefore, the stall force is the essential quantity to characterize polymerization forces.

Cellular force generating structures such as filopodia are made of polymerizing ensembles of interacting actin filaments [5]. Particularly important are bundles of parallel filaments, which can hold together by crosslinking proteins or unspecific attractive interactions. Stall forces of polymerizing actin bundles could be determined experimentally only recently [6].

MTs are tubular filaments, which also consist of an ensemble of typically 13 interacting protofilaments (PFs). The force velocity-relation of polymerizing MTs has been experimentally determined in refs. [3,7], where stall forces around 5 pN have been obtained.

An ensemble of many non-interacting filaments or PFs is believed to have higher stall forces than a single filament because of load sharing effects. First fits of the experimental data on MT growth in ref. [3] were based on the assumption of load sharing and application of ratchet models for a single rigid PF [8]. An explicit continuous model for N rigid PFs in a MT under load resulted in stall forces $\propto N^{1/2}$ [9]. For an analogous discrete growth model of PFs in a MT it has been shown that the stall force of N PFs increases $\propto N$ compared to a single PF [10], in agreement with equal load sharing. Variants of this model which allow a better fit of experimental data were discussed in [11].

In addition to load sharing effects, crosslinking or attractive lateral interactions within filament bundles or between PFs can allow the ensemble to generate even higher forces by exploiting the additional interaction energy [12]. For flexible filaments, zipping mechanisms for force generation can even rely exclusively on attractive interactions [13]. These results suggest that the stall force of interacting filaments or PFs increases by the additional interaction energy per length that a bundle gains upon assembly. Lateral interactions between PFs of a polymerizing MT have been considered in refs. [14–16]. Also for MT growth, approximative analytical results in refs. [14,15] suggest that the stall force of interacting PFs increases by the additional interaction energy per length that the MT gains upon assembly.

Apart from this progress, an exact result for the stall force could not be derived so far. Furthermore, the geometry of the bundle or tube, i.e. the relative positioning of filaments or PFs in the ensemble, has an impact on the mechanics of monomer insertion under load and on the lateral interactions, which are involved.

In this Letter, we investigate the combined effects of at-

tractive filaments interactions and ensemble architecture on the growth kinetics under a compressive force using a discrete growth model [10,14,15]. Based on the concept of polymerization cycles we derive an exact analytical result for the stall force. This result shows that for the discrete model introduced in refs. [10, 14, 15] the stall force is a universal quantity, which only depends on the polymerization energy gain and the interaction strength between filaments or PFs. The stall force is independent of ensemble geometry and independent of the distribution of load force and interaction energy between attachment and detachment rates. The result also shows that the stall force increases $\propto N$, i.e., linearly in the number of filaments.

Using stochastic simulations based on the Gillespie algorithm we find that the growth kinetics below the stall force depends sensitively on the strength of interactions between rigid filaments in a bundle or PFs in a MT *and* on the geometry of the bundle or tube. We find different shapes of the force-velocity relation as well as a complex non-monotonic dependence of the growth velocity on the relative filament positioning. This dependence is very pronounced at low forces well below the stall force but vanishes upon approaching the stall force resulting in a geometry independent stall force.

Our results are of particular interest with respect to the growth kinetics of MTs, which usually contain 13 PFs. Our results imply that a two-start helical structure (with a helical pitch of one tubulin dimer), which is often assumed in modelling, has a distinct force-velocity relation but an identical stall force as the actual three-start helix structure (with a helical pitch of three tubulin monomers) found by electron microscopy [17].

Model and simulation. – We consider a filament consisting of N rigid PFs in a tube-like arrangement such that each PF has two neighbors and periodic boundary conditions apply. For actin bundles, this model neglects effects from thermal shape fluctuations [18] and the existence of defects within the bundle structure [19–21]. Each PF consists of monomers of size d, see fig. 1, The attachment and detachment rates for monomers are k_{on} and k_{off}, respectively, and related to the polymerization energy gain $E_p > 0$ upon adding a monomer by $k_{\text{on}}/k_{\text{off}} = e^{E_p/k_B T}$ at temperature T. For MTs, each monomer is a tubulin dimer, and we will neglect hydrolysis of GTP such that k_{on} and k_{off} are attachment and detachment rates for GTP-tubulin dimers. We also neglect catastrophes and consider MTs only in their growing phase. Effects of hydrolysis are shortly discussed in the end.

Each PF has attractive lateral interactions with its two neighbors; the corresponding lateral association energy (per length) is $\varepsilon_l > 0$. Thus, apart from the polymerization energy, an attaching monomer gains the lateral interaction energy $\varepsilon_l \Delta \ell$, where $\Delta \ell > 0$ is the additional contact length with neighboring monomers, which is created upon inserting the monomer. Likewise, a detaching monomer looses a corresponding interaction en-

ergy resulting in $\Delta \ell < 0$. If the PF can equilibrate its remaining configurational degrees of freedom sufficiently fast during addition or removal of a monomer, thermodynamics requires that lateral interactions change on- and off-rates of that monomer such that $k_{\text{on}}^*/k_{\text{off}}^* = (k_{\text{on}}/k_{\text{off}}) \exp(\varepsilon_l |\Delta \ell|/k_B T)$.

The influence of an external load is described by a force F, which acts only on the leading PF. We denote the position of the tip of the leading filament by x. Insertion of a monomer changes the position of the tip of the leading PF by $\Delta x > 0$ in the on-process, which gives rise to an additional mechanical energy $F \Delta x$. Likewise, removal of a monomer in the off-process gives rise to $\Delta x < 0$. If we assume again that the PF can equilibrate its remaining configurational degrees of freedom sufficiently fast during addition or removal of a monomer under force, thermodynamics requires further modification of on- and off-rates such that [8,9]

$$\frac{k_{\text{on}}^*}{k_{\text{off}}^*} = \frac{k_{\text{on}}}{k_{\text{off}}} e^{(\varepsilon_l |\Delta \ell| - F|\Delta x|)/k_B T}. \qquad (1)$$

If on- and off-rates k_{on}^* and k_{off}^* are specified separately the thermodynamic constraint (1) allows to introduce a load distribution factor θ_F and a lateral energy distribution factor θ_l,

$$
\begin{aligned}
k_{\text{on}}^* &= k_{\text{on}} e^{(-\theta_F F |\Delta x| + (1-\theta_l)\varepsilon_l |\Delta \ell|)/k_B T} \\
k_{\text{off}}^* &= k_{\text{off}} e^{((1-\theta_F) F |\Delta x| - \theta_l \varepsilon_l |\Delta \ell|)/k_B T}. \qquad (2)
\end{aligned}
$$

In general, load and energy distribution factors can depend on the specifics of insertion and removal and differ for each polymerization step. A reasonable assumption is that the external load only affects the on-rate (corresponding to $\theta_F = 1$) and that the on-rate is diffusion-limited and not affected by lateral interactions (corresponding to $\theta_l = 1$) but other choices are thermodynamically possible. In the absence of lateral interactions, this model (with $\theta_F = 1$) was introduced by van Doorn *et al.* [10]. Lateral interactions have been included in refs. [14–16].

The geometry of the bundle or tube has an impact on the mechanics of monomer insertion under load and on the lateral interactions, which are involved. Therefore, we expect a strong influence of geometry on growth kinetics. We control the ensemble geometry by shifting the relative position of neighboring PFs in the initial configuration by a distance h, which we call a *geometry parameter*, see fig. 1. Because of the periodic boundary conditions, we have $N-1$ relative displacements of h between neighboring PFs and one relative displacement of $(N-1)h$. For $h = 0$ we have an aligned or "flat" initial configuration with all PF tips at the same height. For symmetry reasons, geometry parameters h and $-h$ are equivalent. The parameter h can also be shifted by multiple monomer sizes d corresponding to the insertion of additional monomers without changing the kinetics. Therefore, it is sufficient to consider values $0 < h < d/2$. In the following we will measure h in units of d and use $\bar{h} \equiv h/d$.
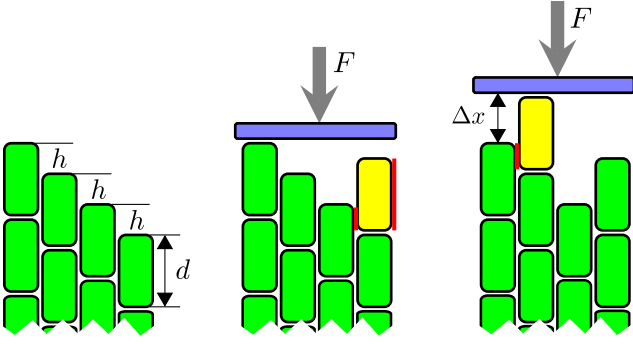
Fig. 1: Schematic picture of the model of interacting PFs polymerizing against the external load force F for $N = 4$. Positions of monomers of size d in neighboring PFs are shifted by the offset h. Insertion of a monomer (yellow) might change the position of the leading PF by Δx (right picture) and create additional contact length with neighboring PFs (red).

Of special interest are MTs, which are usually built from $N = 13$ PFs with tubulin dimers of size $d \simeq 8$ nm [17]. Often it is assumed that MTs with $N = 13$ PFs have an offset $\bar{h} = 1/13$ [10, 11], which results in a symmetric arrangement without a seam in the structure, where the tube closes. The actual structure exhibits a three-start helix with a helical pitch of three tubulin monomers (or $1.5d$) resulting in $\bar{h} = 1.5/13$ [17] and a seam. Other numbers of PFs in MTs ranging from $N = 8$ up to $N = 19$ have been observed as well [17, 22] in the form of two-start or four-start helices corresponding to $\bar{h} = 1/N$ (a helical pitch of d) or $\bar{h} = 2/N$ (a helical pitch of $2d$), respectively. In view of these different possible structures we want to study MT growth kinetics also as a function of the geometry parameter h [14].

In order to simulate the stochastic non-equilibrium growth dynamics of the model we use the Gillespie algorithm [23], which implements a continuous time Markov process with the rates introduced above. For the simulations we use parameters, $k_{\text{on}} = 200$ [1/min], $k_{\text{off}} = 50$ [1/min], a monomer size $d = 8$ nm and a temperature $k_B T = 4.1$pN nm corresponding to room temperature. We used a load distribution factor $\theta_F = 1$ and performed simulations both for energy distribution factors $\theta_l = 0$ (interaction energy affects on-rate) and $\theta_l = 1$ (on-rate diffusion-limited). For each set of parameters, we average over 100 runs.

Polymerization cycles, growth velocity, and stall force. – The polymerization kinetics is completely determined by the configuration of the N PF *ends*: the absolute length of each PF does not enter the rates (2) and we can neglect the possibility of vacancies or holes within a PF, which have not been observed experimentally. Therefore, the growth kinetics can be described by transitions between all possible states of the N PF ends. In general, each such state of the filament end can be described by a

set $\vec{n} = (n_1, ..., n_{N-1})$ of $N - 1$ integer monomer number differences between neighboring PFs with n_i as monomer number difference between PFs i and $i + 1$. Transitions between these states happen by monomer addition and removal with rates (2). Monomer addition (removal) at PF i leads to changes $\Delta n_i = +1$ and $\Delta n_{i-1} = -1$ ($\Delta n_i = -1$ and $\Delta n_{i-1} = +1$). The transition rates $k_{\vec{n}_1, \vec{n}_2}$ between two states $\vec{n}_1$ and $\vec{n}_2$ are only non-zero if both states are related by addition or removal of a single monomer and the corresponding rates are determined by (2), which depend on force and lateral interactions.

During polymer growth, layers of monomers are added and eventually layers with N monomers are completed upon addition of a monomer. After addition of L complete layers the filament end attains the same configuration as initially. Therefore, each completion of L layers closes a *polymerization cycle* C_L of transitions in the network of states $\vec{n}$. A non-zero average polymerization velocity $v = \langle \dot{x} \rangle$ implies that layers are added with a non-zero rate and is equivalent to the existence of *stationary cycle fluxes* in the network of states $\vec{n}$. We can calculate these stationary cycle fluxes using general theorems derived for the kinetics of chemical networks [24–26].

We denote the stationary cycle flux for a polymerization cycle C_L^+ completing L layers by $J(C_L^+)$. Likewise, the opposite cycle removing L layers is called C_L^- and the corresponding stationary flux is $J(C_L^-)$. For an arbitrary cycle $C_L^+ = (\vec{n}_1, \vec{n}_2, ..., \vec{n}_M, \vec{n}_{M+1} \equiv \vec{n}_1)$ of length M and completing L layers ($M \geq NL$), the ratio of stationary cycle fluxes in forward and backward direction is given exactly by the ratio of products of transition rates along the edges of the cycles [24, 26]:

$$\frac{J(C_L^+)}{J(C_L^-)} = \frac{\prod_{i=1}^{M} k_{\vec{n}_i, \vec{n}_{i+1}}}{\prod_{i=1}^{M} k_{\vec{n}_{i+1}, \vec{n}_i}} \tag{3}$$

In addition, we can establish a general relation between the average growth velocity v and the stationary fluxes along cycles C_L: The total stationary net flux along the fundamental set of all cycles C_1 for completions of *single* layers gives the mean time to complete a single layer and, therefore, the mean growth velocity as

$$v = d \sum_{C_1} (J(C_1^+) - J(C_1^-)) \tag{4}$$

Summation over single layer cycles C_1 is sufficient because they form a fundamental set [25], i.e., linear combinations allow to represent cycles for an arbitrary number of L layers.

At the stall force, the growth velocity v vanishes, i.e., $J(C_1^+) = J(C_1^-)$, for all polymerization cycles for single layers. Because such cycles form a fundamental set, it follows that all stationary net polymerization cycle currents have to vanish, i.e., $J(C_L^+) = J(C_L^-)$ for *all* cycles C_L. This leads to the conclusion that the different filament end states are in detailed balance at the stall force, as has

been conjectured in [10]. According to the relation (3) we obtain the following Wegscheider condition [27] for any of the polymerization cycles C_L

$$\prod_{i=1}^{M} \frac{k_{\vec{n}_i,\vec{n}_{i+1}}}{k_{\vec{n}_{i+1},\vec{n}_i}} = 1. \tag{5}$$

which will lead to an exact expression for the stall force.

We first consider the cycle C_L^+. Addition of exactly L layers requires $M_+ = (M + NL)/2$ attachment and $M_- = (M - NL)/2$ detachment transitions, where $M = M_+ + M_-$ and $NL = M_+ - M_-$. Regardless of load and energy distribution factors, the thermodynamic constraint (1) requires

$$\frac{k_{\vec{n}_i,\vec{n}_{i+1}}}{k_{\vec{n}_{i+1},\vec{n}_i}} = \frac{k_{\text{on}}}{k_{\text{off}}} e^{\pm(\varepsilon_l|\Delta\ell_{i,i+1}| - F|\Delta x_{i,i+1}|)/k_B T} \tag{6}$$

for each attachment (+) and detachment (-) transition in C_L^+. Therefore

$$\frac{\prod_{i=1}^{M} k_{\vec{n}_i,\vec{n}_{i+1}}}{\prod_{i=1}^{M} k_{\vec{n}_{i+1},\vec{n}_i}} = \left(\frac{k_{\text{on}}}{k_{\text{off}}}\right)^{M_+ - M_-} e^{(\varepsilon_l|\Delta\ell_M| - F|\Delta x_M|)/k_B T} \tag{7}$$

where $\Delta\ell_M = \sum_{i=1}^{M_+}|\Delta\ell_{i,i+1}| - \sum_{i=1}^{M_-}|\Delta\ell_{i,i+1}| = LNd$ is the total net gain in lateral contact length and $\Delta x_M = \sum_{i=1}^{M_+}|\Delta x_{i,i+1}| - \sum_{i=1}^{M_-}|\Delta x_{i,i+1}| = Ld$ is the total net advance of the leading PF. As a result, we find for the ratio of products of transition rates along the edges of the forward and backward cycles the simple result

$$\frac{\prod_{i=1}^{M} k_{\vec{n}_i,\vec{n}_{i+1}}}{\prod_{i=1}^{M} k_{\vec{n}_{i+1},\vec{n}_i}} = (k_{\text{on}}/k_{\text{off}})^{LN} e^{(\varepsilon_l LNd - FLd)/k_B T} \tag{8}$$

From the condition (5) we then obtain an *exact* expression for the stall force,

$$F_{\text{stall}} = N\left[\varepsilon_l + \frac{k_B T}{d}\ln\left(\frac{k_{\text{on}}}{k_{\text{off}}}\right)\right]. \tag{9}$$

Based on the assumption of detailed balance the same result has also been obtained in ref. [14]. The stall force is a linear function of the number N of filaments in the ensemble and increases linearly with the lateral interaction. It is independent of all load or energy distribution factors of individual polymerization steps. Moreover, the stall force is *independent* of the ensemble architecture. Our derivation shows that geometry independence not only means that the result (9) is independent of the parameter h for an arrangement with constant offset between neighboring PFs but that we obtain the same result (9) for the stall force for completely arbitrary arrangements of PFs relative to each other. Therefore, we also expect the stall force of a bundle of interacting actin filaments not to depend on the precise relative arrangement of actin filaments, which is hard to control in experiments.

In the framework of polymerization cycles the so-called one-layer approximation introduced in [15] is equivalent to a "one-cycle" approximation, which restricts the sum in (4) to a contribution from a single cycle dominating the sum in the limit of large forces close to the stall force. Therefore, the exact expression (9) for the stall force, at which all cycle currents become zero, is also recovered in the one-layer approximation in ref. [15]. This indicates how a systematic improvement of the one-layer approximation could be achieved by inclusion of more polymerization cycles, which will leave the result (9) for the stall force unaffected.

Experimentally, force-velocity curves have been measured [3,7] but the stall force is not directly accessible. Nevertheless, an exact result such as (9) can help to constrain the analysis of experimental data.

We conclude this section with a short discussion of the effects of GTP-hydrolysis on the stall force of MTs. GTP-tubulin attaches and can hydrolyze within the MT to GDP-tubulin, which gives rise to different off-rates $k_{\text{off,T}}$ and $k_{\text{off,D}}$ for GTP and GDP monomers, respectively. This leads to a coupling between polymerization cycles and hydrolysis, if the probability p_D that a monomer at the filament end is of GDP-type becomes non-zero. For small probabilities p_D, effects from hydrolysis can be included approximately by using an effective off-rate $k_{\text{off,eff}} = p_T k_{\text{off,T}} + p_D k_{\text{off,D}}$ in the result (9) for the stall force, where $p_T = 1 - p_D$ is the probability that a monomer at the filament end is of GTP-type. Because hydrolysis destabilizes the filament and $k_{\text{off,T}} < k_{\text{off,D}}$, hydrolysis will generally *reduce* the stall force. For single actin filaments, the effect of hydrolysis on the force-velocity relation has been calculated in ref. [28]. Hydrolysis and a non-zero p_D also give rise to catastrophes as soon as the entire GTP-cap of a MT becomes hydrolyzed.

Simulation results. – In simulations we can explore not only the stall force but the full force-velocity relation. We characterize the growth process by the average growth velocity $v = \langle\dot{x}\rangle$. We determine the force-velocity relation as a function of *both* the PF interaction (per length) ε_l *and* the geometry parameter h. From the force-velocity curves, we determine the stall force numerically and investigate how the stall force depends both on PF interactions and geometry parameter. Some of our simulation results have also been obtained in ref. [14] using a fixed time step Monte-Carlo algorithm.

Force-velocity relation. We first describe results for the force-velocity relation of $N = 13$ PFs corresponding to a MT using the rates (2). The shape of the force-velocity relation depends on the PF interaction ε_l [15,16]. For $\varepsilon_l = 0$ all force-velocity curves end at the same velocity $v(0) = d(k_{\text{on}} - k_{\text{off}})$ for zero force, independently of the geometry parameter h, see fig. 2a. Simulations confirm that force-velocity curves for different geometry parameters h exhibit the same stall force $F_{\text{stall}} = N(k_B T/d)\ln(k_{\text{on}}/k_{\text{off}})$ as predicted in eq. (9). The shape of the force-velocity curves between $F = 0$ and the stall force $F = F_{\text{stall}}$, however, depends on the geometry parameter h, as shown in
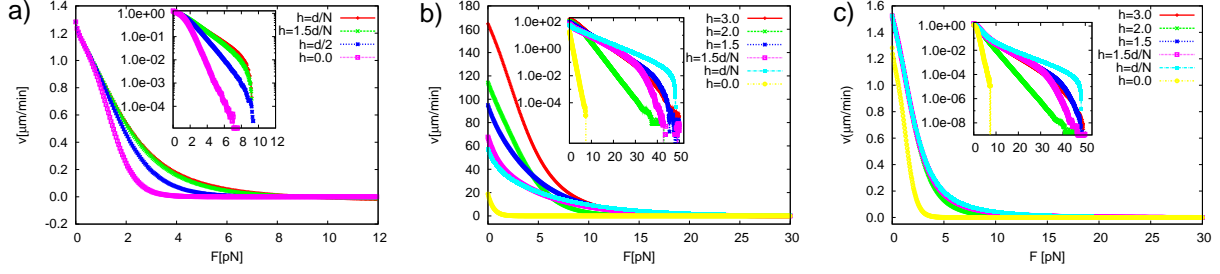
Fig. 2: Geometry-dependence of the force-velocity relation for $N = 13$ PFs and two different values of the lateral interaction, (a) $\varepsilon_l = 0pN$ (curves are independent of the energy distribution factor θ_l) and (b),(c) $\varepsilon_l = 3.0pN$, ((b) $\theta_l = 0$, (c) $\theta_l = 1$). For each lateral interaction, different geometry parameters h (in units of nm and for monomer size $d = 8$nm) are compared. Insets are logarithmic plots.

fig. 2a: for forces $F > 0$ and small h, the kinetically limiting step is the insertion of the first monomer to an almost flat configuration. This rate-limiting step becomes faster for increasing h because the increase Δx of the leading tip becomes smaller. This results in steeper force-velocity curves for decreasing values of the geometry parameter h, as can be seen in fig. 2a.

For $\varepsilon_l > 0$, also the velocities at zero force $v(0)$ depend on the geometry parameter h and on the energy distribution factor θ_l. For increasing h, the zero-force velocity $v(0)$ increases because the attractive PF interaction accelerates growth by reducing the off-rate (for $\theta_l = 1$, see fig. 2(c)) or increasing the on-rate (for $\theta_l = 0$, see fig. 2(b)). Increasing the on-rate ($\theta_l = 0$) leads to a much stronger effect. On the other hand, the simulations confirm that the stall force remains identical for different geometry parameters h and for the different energy distribution factors θ_l in fig. 2(b) and $\theta_l = 0$ in fig. 2(c) as predicted by eq. (9). Nevertheless, it is not possible to simply conclude that force-velocity curves become increasingly steep for increasing geometry parameter h. Only for $h = 0$, strong suppression of the rate-limiting first insertion step by force always results in the steepest force-velocity curves, see fig. 2. Then, the stall force is hard to determine because the force-velocity curve is extremely flat with measured zero velocity over a range of higher forces.

Stall force. It is possible to directly check the above exact analytical result (9) for the stall force in simulations by the condition $v(F_{\text{stall}}) = 0$, i.e., by determining the force where the average growth velocity in the simulation vanishes. In simulations this is done by applying a linear interpolation to data points of force-velocity curves in vicinity of the stall force.

In fig. 3 we show the simulation results for the stall force as a function of the lateral interaction ε_l for (a) $N = 13$ and different values of the geometry parameter h and for (b) fixed h and different values of N. The simulation results clearly show a linear increase with ε_l and N and confirm the analytical result (9). In particular, we find no dependence on the geometry parameter h.
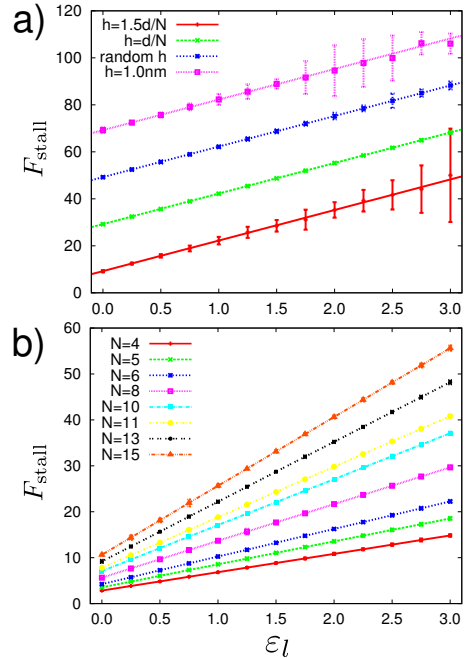

Fig. 3: Stall force (in pN) as a function of lateral interaction energy ε_l (in pN) for $\theta_l = 1$. Points represent simulation results, lines the analytical result (9). (a) For $N = 13$ PFs and different geometry parameters $h = \frac{3}{2}d/N \approx 0.934$nm, $h = d/N \approx 0.615$nm, random h, $h = 1.0$nm (from bottom to top). Curves are shifted by 0, 20, 40 and 60 nm respectively. (b) For a geometry parameter $h = d/N$ and different PF numbers $N = 4,5,6,8,10,11,13$ and 15 (from bottom to top).

The derivation of (9) was not limited to PF arrangement with a *constant* offset h between neighboring PFs but predicts the same stall force for completely arbitrary arrangements of PFs. We checked this prediction by simulations of several random arrangements with random displacements between neighboring filaments, see fig. 3a (green line).

Dependence of velocity on the geometry parameter. The simulations allow us to explore how the growth veloc-
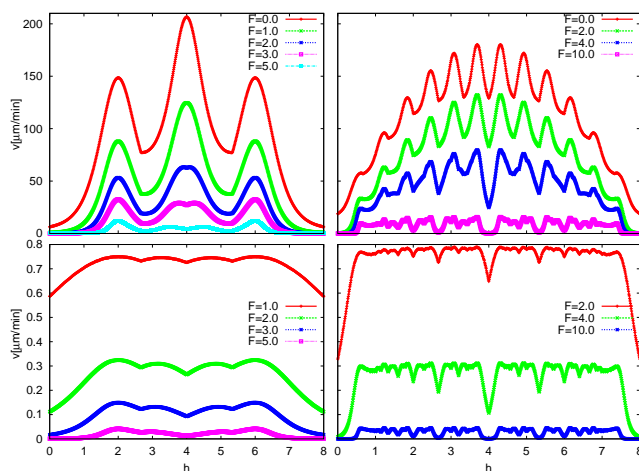
Fig. 4: Growth velocity as a function of the geometry parameter h (in nm and for monomer size $d = 8$nm) for $N = 4$ (left) and $N = 13$ (right) PFs for different values of the force F (in pN). The lateral interaction energy is $\varepsilon_l = 3.0$pN and the lateral energy distribution factor $\theta_l = 1$ for both top pictures and $\theta_l = 0$ for both bottom pictures. For vanishing force $F = 0$ the curves exhibit $N - 1$ maxima at $\bar{h} = i/N$ with $i = 1, .., N - 1$. With increasing force, some maxima vanish and new maxima can emerge.

ity v depends on the geometry parameter $\bar{h}$ ($0 < \bar{h} < 1$) for different load forces F, see fig. 4. The curves $v(\bar{h})$ are symmetric with respect to the axis $\bar{h} = 1/2$. For $\varepsilon_l > 0$ and zero load force $F = 0$, the curves $v(\bar{h})$ exhibit $N - 1$ maxima corresponding to relative displacements $\bar{h} = i/N$ with $i = 1, .., N - 1$. At these values of $\bar{h}$, the relative displacement h is commensurate with the monomer size d such that polymerization cycles are possible, where all subsequently attached monomers gain the same lateral interaction energy. This avoids rate-limiting attachment steps and leads to optimal polymerization velocities. The maxima are very pronounced for energy distribution factors $\theta_l = 0$, where the on-rate is exponentially increased by lateral interactions and rather broad plateaus for $\theta_l = 1$. This implies that MT models using $\bar{h} = 1/13$ [10,11] overestimate the growth velocity as compared to the actual three-start helix with $\bar{h} = 1.5/13$.

With increasing load F the height of the maxima decreases, maxima can vanish or become minima, and new local maxima can appear. Upon approaching the stall force $F \approx F_{\text{stall}}$, all curves $v(\bar{h})$ become flat, which supports the analytical result of an h-independent stall force.

Conclusion. – Based on the concept of polymerization cycles we obtained the exact result (9) for the stall force of polymerizing ensembles of rigid protofilaments with lateral interactions. The stall force is a linear function of the number N of filaments in the ensemble and increases linearly with the lateral interaction. On the other hand, the stall force is independent of the geometry of the

ensemble and load or energy distribution factors. These results have been confirmed by simulations using the Gillespie algorithm. Simulations also show that the shape of the force-velocity relation exhibits a pronounced dependence on the ensemble geometry below the stall force. Our results are relevant for the interpretation of experimental data on the force-velocity relation in microtubule polymerization and in the polymerization of bundles of interacting actin filaments or microtubules.

REFERENCES

[1] Bray D., *Cell Movements: From Molecules to Motility* (Garland Publishing) 2001
[2] Mogilner A., *Curr. Opin. Cell Biol.*, **18** (2006) 32.
[3] Dogterom M. and Yurke B., *Science*, **278** (1997) 856.
[4] Hill T.L., *Linear aggregation theory in cell biology* (Springer) 1987
[5] J.Faix and K.Rottner, *Curr. Opin. Cell Biol.*, **18** (2006) 18.
[6] Footer M.J.,Kerssemakers J.W.J., Theriot J.A. and Dogterom M., *Proc. Nat. Acad. Sci. USA*, **104** (2007) 2181.
[7] Janson M. and Dogterom M., *Phys. Rev. Lett.*, **92** (2004) 248101.
[8] Peskin C.S., Odell G.M. and Oster G.F., *Biophys. J.*, **65** (1993) 316.
[9] Mogiler A. and Oster G., *Eur. Biophys. J.*, **28** (1999) 235.
[10] van Doorn G.S., Tănase C., Mulder B.M. and Dogterom M., *Eur. Biophys. J.*, **29** (2000) 2.
[11] Kolomeisky A.B. and Fisher M.E., *Biophys. J.*, **80** (2001) 149.
[12] L.Mahadevan and P.Matsudaira, *Science*, **288** (2000) 95.
[13] Kühne T., Lipowsky R. and Kierfeld J., *EPL*, **86** (2009) 68002.
[14] Tanase C., *Physical Modeling of Microtubule Force Generation and Self-Organization,* PhD Thesis, Wageningen University, 2004.
[15] Stukalin E.B. and Kolomeisky A.B., *J. Chem. Phys.*, **121** (2004) 1097.
[16] Son J., Orkoulas G. and Kolomeisky A.B., *J. Chem. Phys.*, **123** (2005) 124902.
[17] Li H., DeRosier D.J., Nicholson W.V., Nogales E. and Downing K.H., *Structure*, **10** (2002) 1317.
[18] Kierfeld J., Kühne T. and Lipowsky R., *Phys. Rev. Lett.*, **95** (2005) 038102.
[19] Gov N., *Phys. Rev. E*, **78** (2008) 011916.
[20] Yang Y., Meyer R.B. and Hagan M.F., *Phys. Rev. Lett.*, **104** (2010) 258102.
[21] Grason G., *Phys. Rev. Lett.*, **105** (2010) 045502.
[22] Chretien D. and Wade R.H., *Biol. Cell*, **71** (1991) 161.
[23] Gillespie D.T., *J. Chem. Phys.*, **28** (1977) 395.
[24] Hill T.L., *Journal of theoretical biology*, **10** (1966) 442.
[25] Schnakenberg J., *Rev. Mod. Phys.*, **48** (1976) 571.
[26] Hill T.L., *Free energy transduction and biochemical cycle kinetics* (Springer) 1989
[27] Wegscheider R., *Z. Phys. Chem.*, **39** (1901) 257.
[28] Ranjith P., Lacoste D., Mallick K. and Joanny, J.-F., *Biophys. J.*, **96** (2009) 2146.